Stroboscopic observation of quantum many-body dynamics

Stefan Keßler,[1] Andreas Holzner,[2] Ian P. McCulloch,[3] Jan von Delft,[2] and Florian Marquardt[1,4]
[1]*Institute for Theoretical Physics, Universität Erlangen-Nürnberg, Staudtstr. 7, 91058 Erlangen, Germany*
[2]*Physics Department, Arnold Sommerfeld Center for Theoretical Physics, and Center for NanoScience, Ludwig-Maximilians-Universität München, D-80333 München, Germany*
[3]*School of Physical Sciences, The University of Queensland, Brisbane, QLD 4072, Australia*
[4]*Max Planck Institute for the Science of Light, Günter-Scharowsky-Straße 1/Bau 24, 91058 Erlangen, Germany*

Recent experiments have demonstrated single-site resolved observation of cold atoms in optical lattices. Thus, in the future it may be possible to take repeated snapshots of an interacting quantum many-body system during the course of its evolution. Here we address the impact of the resulting Quantum (anti-)Zeno physics on the many-body dynamics. We use time-dependent DMRG to obtain the time evolution of the full many-body wave function that is then periodically projected in order to simulate realizations of stroboscopic measurements. For the example of a 1-D lattice of spin-polarized fermions with nearest-neighbor interactions, we find regimes for which many-particle configurations are stabilized and destabilized depending on the interaction strength and the time between observations.

Introduction.— In the last years ultracold atoms in optical lattices have proven to be a versatile tool to study various quantum many-body phenomena [1, 2]. Recently, tremendous progress has been achieved by implementing single-site resolved detection [3, 4] and addressing [5] of atoms. This opens the path for investigating the evolution of non-equilibrium quantum many-body states by taking snapshots revealing the position of each single atom. For simpler systems, the effect of frequent observations on the decay of an unstable state (or the dynamics of a coherently driven transition) has already been discussed and observed, leading to the notion of the Quantum (anti-)Zeno effect [6–9]. Zeno physics has also been seen in cold-atom experiments with atomic loss channels [10] and was theoretically addressed in [11–13]. Experiments with single-site detection, however, would allow to explore the effect of observations on the dynamics of a truly interacting quantum many-body system. Here we exploit a numerically efficient approach to simulate the repeated observation of many-particle configurations in interacting lattice models. This represents an idealized version of the dynamics that may be realized in future experiments. We illustrate the main features of this "stroboscopic" many-body dynamics in the case of a 1-D lattice of spin-polarized fermions with nearest-neighbor interactions. We find a variant of the Quantum Zeno Effect and discuss its tendency to inhibit or accelerate the break-up of certain many-particle configurations. Interestingly, the lifetime of such particle clusters depends in a non-monotonous fashion on the time interval between observations. These features may be seen, for example, in the expansion dynamics of interacting atomic clouds in a lattice.

Technique.— Ideally, each observation is a projective measurement in the basis of many-particle configurations (occupation number states in real space). However, due to the exponentially large number of states, we need a numerically efficient way to sample such outcomes. We start by drawing the position of the first particle from a random distribution given by the one-particle density. Afterwards, we draw the position of the second particle, *conditioned* on the location of the first one, and proceed iteratively. In doing so, we build on the fact that the n-particle density ρ_n factorizes into conditional probabilities,

$$\rho_n(s_1,\ldots,s_n) = \rho_1(s_1)\cdot\prod_{i=2}^{n}\rho_i(s_i|s_{i-1},\ldots,s_1), \qquad (1)$$

where s_i denotes the position of the ith particle and $\rho_i(s_i|s_{i-1},\ldots,s_1)$ is the conditional probability of finding the ith particle at site s_i given that there are $i-1$ particles at the sites $s_1,\ldots,s_{i-1}$. Using this approach, only $n\cdot N_s$ values of joint probability densities have to be calculated, in comparison to the full number $\binom{N_s}{n}$ of possible many-body configurations. This approach relies on being able to calculate efficiently both the pure time evolution between observations and the i-particle densities ($1\le i\le n$). For the present work, we use the time-dependent DMRG [14–17], which is an extremely powerful method for interacting 1-D systems. For the fermionic model considered below, it is numerically even more efficient to draw the position of the first particle as before and then project the state onto those configurations where a particle is present at the selected site. After rescaling the resulting state, the new one-particle density is calculated. From this distribution we draw the position of the second fermion, excluding all sites already occupied by a fermion, and iterate the steps for the remaining fermions.

Model.— In this paper, we study spin-polarized fermions in a 1-D lattice governed by the Hamiltonian

$$\hat{\mathcal{H}} = -J\sum_i\left(\hat{c}_i^\dagger\hat{c}_{i+1}+h.c.\right)+V\sum_i\hat{n}_i\hat{n}_{i+1}\,. \qquad (2)$$

Here, $\hat{c}_i(\hat{c}_i^\dagger)$ denote fermionic destruction (creation) operators on lattice site i, and $\hat{n}_i$ is the particle number. The

first term describes hopping with amplitude J between neighboring sites, the second encodes the interaction between fermions at neighboring sites. The Hamiltonian displays a dynamical $V \mapsto -V$ symmetry which shows up in expansion experiments [18]. Following analogous steps as in [18], we can conclude: If both the initial state and the experimentally measured quantity $\hat{\mathcal{O}}$ are invariant under both time reversal and π–boost, the observed time evolution $\langle\hat{\mathcal{O}}(t)\rangle$ is identical for repulsive and attractive interaction of the same strength. Here, a π–boost refers to a translation of all momenta by π. The initial occupation number states and the n-particle density observables in our case fall within the scope of this theorem. Thus, the only relevant dimensionless parameters in our scenario are $|\frac{V}{J}|$ and the rescaled time between observations, $J\Delta t$.

Single particle.—We first briefly turn to the single-particle case, with $V = 0$ in Eq. (2). This leads to a tight-binding band $E(k) = -2J\cos(k)$. A particle located initially at a single site is in a superposition of all plane wave momenta $k = -\pi \ldots \pi$. After a time t, the probability of detecting it at a distance l from the initial site is $\rho(l,t) = \mathcal{J}^2_{|l|}(2Jt)$, where $\mathcal{J}$ is the Bessel function of the first kind. This is shown in Fig. 1(a). The particle moves ballistically, with $\langle l^2\rangle = 2(Jt)^2$. When the particle is observed stroboscopically, at intervals Δt, the ballistic motion turns into diffusion. In this case, after m time steps of duration $\Delta t = t/m$, we have $\langle l^2\rangle = 2J^2 t\,\Delta t$. Thus the motion slows down, and in the limit of an infinite observation rate ($\Delta t \to 0$), the particle is frozen, which is known as the Quantum Zeno effect.

Dynamics of non-interaction fermions.— After each observation, the many-particle wave function is a Slater determinant of single particle wave functions, and for non-interacting fermions this remains true even during the subsequent evolution. Using Wick's theorem, the n-particle density of these N fermions can be written as (see also [19]):

$$\rho_n(s_1,\ldots,s_n;t) = \frac{(N-n)!}{N!}\begin{vmatrix} M_{s_1 s_1} & \ldots & M_{s_1 s_n} \\ \ldots & & \ldots \\ M_{s_r s_n} & \ldots & M_{s_n s_n} \end{vmatrix}. \quad (3)$$

Here, $M_{s_k s_l} = \sum_{j=1}^{N} T_{s_k m_j}(t) T^*_{s_l m_j}(t)$, where $T_{kl}(t) = i^{(k-l)}\mathcal{J}_{k-l}(2Jt)$ is the propagator for one fermion, and the sum is taken over all sites m_j that were occupied at the initial time. The normalization is chosen such that $\sum_{s_1,\ldots,s_n}\rho_n(s_1,\ldots,s_n;t) = 1$. Note that the one-particle density ρ_1 is just the sum of the individual densities (Fig. 1b). Motion in arbitrary potentials would be captured by different propagators T_{kl}.

Numerical details.— For the interacting case to be discussed now, we use a tDMRG simulation, with time steps of $J\delta t = 0.1$, a lattice of typically 115 sites, and keeping up to approximately 1000 states, at a truncation error of 10^{-6}. The n-particle densities are evaluated by calculating expectation values of the tDMRG wave functions. For the non-interacting case we checked the tDMRG density against the exact formula (3) for times $Jt \leq 20$. Note that tDMRG has been employed for dissipative dynamics of cold atoms recently [20].

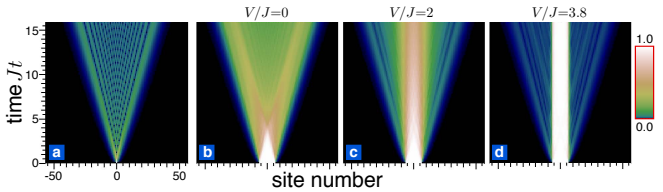

Fig. 1. Time evolution of the density profile of fermions expanding in a lattice without observation. (a) Single fermion for comparison. (b-d) Expansion of 13 fermions initially located at adjacent lattice sites for increasing interaction strength.

Stroboscopic many-body dynamics.— We will focus on an experimentally interesting scenario, namely the expansion of an interacting cloud from an initially confined state. Such an expansion in 2D was observed in an experiment with 2-species fermions in [18]. We will first briefly address the evaporation itself and then discuss qualitatively the resulting stroboscopic dynamics, with a more refined analysis presented further below. Fig. 1(b-d) shows the effect of the interaction on the free (unmeasured) time evolution of the density profile. For increasing interaction the fermions tend to remain localized near their initial positions. For large interaction strengths $|V/J| \gtrsim 3$ and the times shown here, $tJ < 16$, a more detailed analysis reveals that evaporation proceeds via the rare event of a single fermion dissociating from the cluster. This particle then moves away ballistically. The evaporation of particles off the edge of the confined cloud is hindered by the formation of bound states. This is a crucial phenomenon we will also encounter in the context of repeated measurements. For smaller interaction strengths ($|V/J| \lesssim 2$), the fermions split gradually into a larger and larger number of clusters as time increases. The parameter regimes in which the model described by Eq. (2) exhibits diffusive or ballistic transport was addressed using tDMRG in [21]. The effects of stroboscopic observation are shown in Fig. 2, for typical realizations of this stochastic process. For non-interacting fermions we find the behavior expected from the single particle case. The spread (and thus, the diffusion constant) increases with larger observation time intervals Δt. For very small $J\Delta t$ (strong Zeno effect), the motion is diffusive with a small diffusion constant that becomes independent of $|V/J|$. In general, it is useful to discuss the "lifetime" of the initial inner cluster that evaporates via expansion. For the interacting case, the lifetime is shortest at some intermediate observation time interval Δt, while it is enhanced again for large Δt. Apparently, at very large $|V/J|$, the lifetime may have yet another local

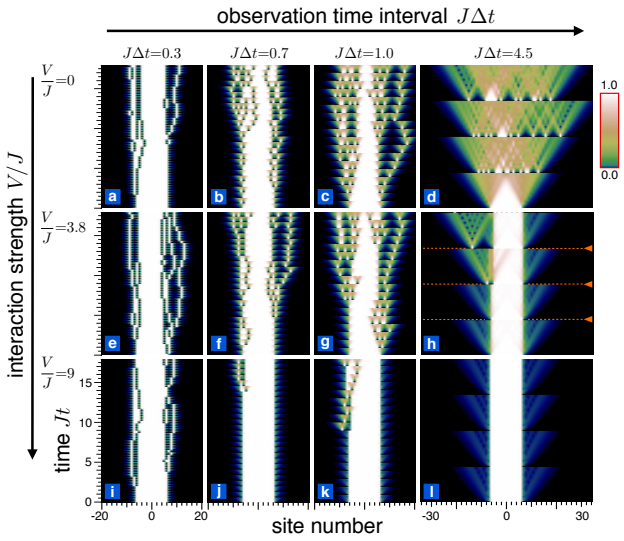

Fig. 2. Density plot of specific realizations for the expansion of 13 fermions with site-resolved detection during the evolution. We show the full evolution of density even between observations, which collapse the many-body wavefunction at regular time intervals $J\Delta t$ (as indicated by the dashed lines in panel h). Without interaction (a-d) the lifetime of the initial configuration decreases for larger $J\Delta t$, while for large interaction the lifetime is shortest for intermediate observation times $J\Delta t$ (h,l). For small $J\Delta t$ the dynamics becomes independent of $|V/J|$, see (a,e,i).

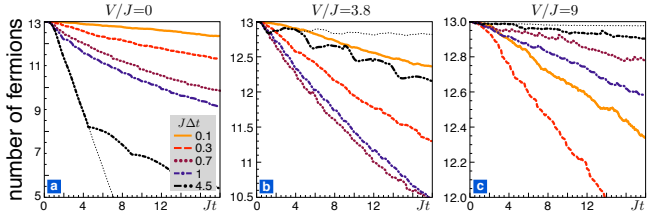

Fig. 3. For the parameters of Fig. 2, each panel shows the average number of fermions remaining at the 15 central lattice sites as a function of evolution time t for different values of $J\Delta t$. The thin dotted line corresponds to an evolution without observation. (a) Without interactions, the lifetime decreases monotonically with increasing $J\Delta t$. (b) At $V/J = 3.8$, the lifetime increases again for large $J\Delta t$. (c) At large interactions, $V/J = 9$, the lifetime is non-monotonous even for intermediate $J\Delta t$; compare $J\Delta t = 0.3, 0.7, 1.0$. Note that the lifetimes in (a-c) are almost identical for $J\Delta t = 0.1$.

maximum for intermediate Δt, see Fig. 2(j). We confirm this striking non-monotonous behavior of the lifetime by simulating 400 realizations for each panel shown in Fig. 2 and plot the average number of fermions at the central 15 lattice sites as a function of time, in Fig. 3. For sufficiently large $J\Delta t$ and $|V/J|$, this number decays roughly linearly at a rate that sets the inverse lifetime.

We will now see that the features observed here can be mainly attributed to two ingredients: a bound state and the two-level dynamics between the initial state and the state with a fermion detached from the others.

Doublets and the role of interactions.— The effect of interactions can be discussed already for the stroboscopic dynamics of two fermions. We focus on the decay of a doublet, i.e. two fermions sitting at neighboring sites.

In the quantum Zeno limit, $J\Delta t \ll 1$ (or $J\Delta t \ll |2J/V|$ for large $|V|$, see below) only single hopping events occur during Δt. The probability for a fermion hopping left or right during Δt is $2(J\Delta t)^2$. This leads to a rate equation for the probabilities p_l to find the two fermions l sites away from each other:

$$\frac{d}{dt}\,p_l = 2J^2\Delta t\,[p_{l+1} - p_l + (1-\delta_{l,1})(p_{l-1} - p_l)]\ . \quad (4)$$

In this limit, the average decay time for a doublet is $\langle Jt\rangle = 1/2J\Delta t$, independent of V, compare with Fig. 2 (a,e,i).

For larger $J\Delta t$, the interaction will become important. It gives rise to a bound state when the particles come close to each other (this effect also exists for clusters of more particles [22]). It is convenient to separate the dynamics of the 2-particle states into relative and center-of-mass (c.o.m.) motion. Considering the basis $|l, K\rangle = \frac{1}{\sqrt{\mathcal{N}}}\sum_j \exp\{iK[j+l/2]\}c_j^\dagger c_{j+l}^\dagger|vac\rangle$ of the 2-particle sector with relative coordinate l, center of mass coordinate $j+l/2$, and total wavenumber $K = k_1 + k_2$, the action of the Hamiltonian (2) is $\mathcal{H}|l,K\rangle = |K\rangle \otimes \mathcal{H}_K|l\rangle$. The first part describes a plane wave with c.o.m. wavenumber K, the second the relative motion, which is described by an effective Hamiltonian

$$\mathcal{H}_K|l\rangle = -2J_K\big[|l+1\rangle + (1-\delta_{l,1})|l-1\rangle\big] + V\delta_{l,1}|l\rangle, \quad (5)$$

with a hopping amplitude $J_K = J\cos(K/2)$ depending on K. We now discuss the decay of a doublet (see Fig. 4(a)) with the help of the doublet survival probability $P_D(t) = \sum_{L'}|\langle l=1, L'|e^{-iHt}|l=1, L\rangle|^2$, where L and L' are c.o.m coordinates. A bound state exists if $|V| \geq |2J_K|$. It is given by $|\psi_K\rangle \propto \sum_{l=1}^{\infty}(-J_K/V)^{l-1}|l\rangle$. In the absence of observations the doublet survival probability is for $t\to\infty$ given by $P_D(\infty) = \frac{1}{2\pi}\int_{-\pi}^{\pi} dK\,|\langle\psi_K|l=1\rangle|^4$. Specifically, in the more interesting case of large $|V/2J| \geq 1$, we have

$$P_D(\infty) = 1 - (2J/V)^2 + \frac{3}{8}\,(2J/V)^4\ . \quad (6)$$

While $P_D(\infty)$ is determined by the bound state, the evolution for times $Jt < 1$ is mostly determined by the two-level dynamics connecting $|l=1\rangle$ and $|l=2\rangle$. In this short-time limit, we find

$$P_D(t) = 1 - \frac{1}{\pi}\int_0^{\pi} dK\,\frac{\cos^2(K/2)}{\xi_K^2}\sin^2(2J\xi_K t), \quad (7)$$

with $\xi_K = \sqrt{(\frac{V}{4J})^2 + \cos^2(K/2)}$ (note the integral over K). In the strongly interacting regime we find three

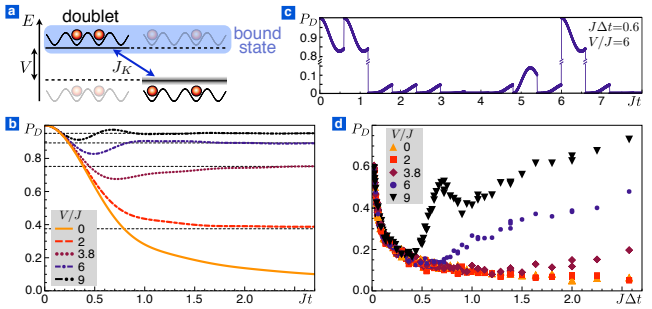

Fig. 4. (a) Doublet decay level scheme. The doublet is separated from the continuum of unbound states by an energy gap V. (b) Probability P_D of finding the doublet intact after an evolution time Jt. Dashed black lines correspond to $P_D(\infty)$ found in Eq. 6. (c) Single trajectory of P_D for a time evolution subject to observations, with $J\Delta t = 0.6$ and $V/J = 6$. (d) Doublet survival probability P_D as function of the observation time interval $J\Delta t \geq 0.02$ for a fixed total evolution time $Jt = 18$. Note the non-monotonous dependence on $J\Delta t$ for finite interactions.

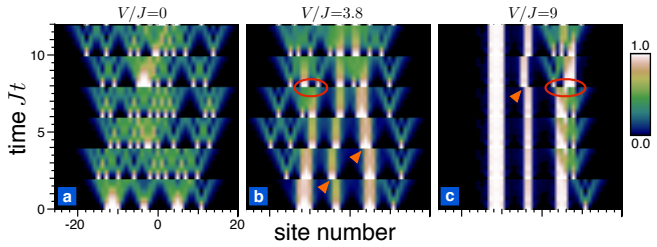

Fig. 5. Density plot for the time evolution of an initial state with clusters of different numbers of fermions and observations with time steps $J\Delta t = 2$. (b,c) For large interaction strength we find clusters moving as a whole (indicated by triangles). Also processes with single fermions being exchanged between clusters or attached to a new cluster are observed, indicated by loops.

regions for the doublet survival probability: for times $Jt \ll \xi_{K=0}^{-1}$ the probability is independent of the interaction strength, $P_D(t) = 1-2(Jt)^2$, for times $\xi_{K=0}^{-1} < Jt < 1$ one expects an oscillating behavior of $P_D(t)$ given by Eq. (7) with a period approximately $\frac{2\pi}{V}$ for $|V/4J| \gg 1$, and for $Jt \gg 1$ the probability approaches $P_D(\infty)$.

The full evolution of $P_D(t)$ using exact diagonalization is shown in Fig. 4. Without observations (Fig. 4(b)), $P_D(t)$ is interaction-independent at small times $Jt \lesssim 0.2$. Temporal oscillations in P_D develop for higher interaction strengths ($V/J \gtrsim 3.5$). The non-monotonic behavior at small times suggests that a change of the observation time interval in the stroboscopic dynamics may have a drastic effect on the survival probability. This effect is confirmed in Fig. 4(d). In that figure, the observation time interval $J\Delta t$ is varied, while keeping the total evolution time constant, $Jt = 18$ (with a corresponding number of observations $t/\Delta t$). The stroboscopic evolution is interaction-independent up to times $J\Delta t = \frac{\pi}{V/J}$. For larger $J\Delta t$ there is a drastic recovery of P_D, which can show oscillations as a function of Δt. The qualitative behavior matches well the expectations from Fig. 4(b) and does not depend in detail on the total time t. Thus we have explained the most prominent features of the stroboscopic many-body dynamics, shown in Fig. 2 and Fig. 3, through our the discussion of the doublet.

Other features that can be observed in the stroboscopic dynamics are the motion of whole clusters of fermions through the lattice and the exchange of fermions between clusters, as shown in Fig. 5. As expected, clusters are very stable for high interaction strengths. The hopping amplitude for a cluster of n fermions is of order $J^n/|V|^{n-1}$, decreasing strongly for larger clusters, as can be perceived in Fig. 5(c).

Experimental realization and outlook.— Our choice of Hamiltonian was primarily dictated by simplicity, as a one-species fermionic model in 1D. This Hamiltonian is related to the Heisenberg XXZ model by Wigner-Jordan transformation. The stroboscopic dynamics is identical for both models as the outcome of observations depends only on spatial density-density correlations. These Hamiltonians can be experimentally realized in optical lattices with fermionic polar molecules [23] or 2-species fermions in the insulating phase [24]. For both realizations single-site detection has not yet been implemented, but ideas exists and experimental progress is being made towards this goal. The generic features discussed in this paper should be found as well in other model, e.g. the Bose-Hubbard model (where a double occupancy would correspond to the doublet state). Experimentally, the most challenging step needed to observe the interplay of many-body dynamics and measurements discussed here would be to make the observations non-destructive, whereas currently atoms are heated into higher site orbitals. Beyond the scenarios discussed here, one may also be interested in the influence of external driving or measurements that are either weak or target only specific sites.

Acknowledgments.— Financial support by the DFG through NIM, SFB/TR 12, and the Emmy-Noether program is gratefully acknowledged.

[1] I. Bloch, J. Dalibard, and W. Zwerger, Rev. Mod. Phys. **80**, 885 (2008).
[2] M. Lewenstein *et al.*, Adv. Phys. **56**, 243 (2007).
[3] W. S. Bakr *et al.*, Nature Physics **462**, 74 (2009).
[4] J. F. Sherson *et al.*, Nature **467**, 68 (2010).
[5] C. Weitenberg *et al.*, arXiv:1101.2076v1.
[6] B. Misra and E. C. G. Sudarshan, J. Math. Phys. (N.Y.) **18**, 756 (1977).
[7] W. M. Itano *et al.*, Phys. Rev. A **41**, 2295 (1990).
[8] M. C. Fischer, B. Gutiérrez-Medina, and M. G. Raizen, Phys. Rev. Lett. **87**, 040402 (2001).

[9] P. Facchi and S. Pascazio, J. Phys. A: Math. Theor. **41**, 493001 (2008), and references therein.
[10] N. Syassen *et al.*, Science **320**, 1329 (2008).
[11] J. J. García-Ripoll *et al.*, New J. Phys. **11**, 013053 (2009).
[12] A. J. Daley *et al.*, Phys. Rev. Lett. **102**, 040402 (2009).
[13] R. Schützhold and G. Gnanapragasam, Phys. Rev. A **82**, 022120 (2010).
[14] G. Vidal, Phys. Rev. Lett. **93**, 040502 (2004).
[15] A. J. Daley *et al.*, J. Stat. Mech. (2004) P04005.
[16] S. R. White and A. E. Feiguin, Phys. Rev. Lett. **93**, 076401 (2004).
[17] P. Schmitteckert, Phys. Rev. B **70**, 121302(R) (2004).
[18] U. Schneider *et al.*, arXiv:1005.3545v1.
[19] G. Rickayzen, *Green's Functions and Condensed Matter* (Academic Press, New York, 1980).
[20] H. Pichler, A. J. Daley, and P. Zoller, Phys. Rev. A **82**, 063605 (2010).
[21] S. Langer *et al.*, Phys. Rev. B **79**, 214409 (2009).
[22] B. Sutherland, *Beautiful Models* (World Scientific, 2004).
[23] H. P. Büchler, A. Micheli, and P. Zoller, Nature Physics **3**, 726 (2007).
[24] L.-M. Duan, E. Demler, and M. D. Lukin, Phys. Rev. Lett. **91**, 090402 (2003).